V International Conference on Computational Methods for Coupled Problems in Science and Engineering
COUPLED PROBLEMS 2013
S. Idelsohn, M. Papadrakakis and B. Schrefler (Eds)

MASS PRESERVING DISTRIBUTED LANGRAGE MULTIPLIER APPROACH TO IMMERSED BOUNDARY METHOD

DANIELE BOFFI*, NICOLA CAVALLINI*, FRANCESCA GARDINI* AND LUCIA GASTALDI†

*Dipartimento di Matematica "F. Casorati"
Università degli Studi di Pavia
Via Ferrata 1, 27100 Pavia, Italy
{daniele.boffi,nicola.cavallini,francesca.gardini}@unipv.it

†DICATAM
Dipartimento di Ingegneria Civile, Architettura, Territorio, Ambiente e di Matematica
Università degli Studi di Brescia
via Branze 43, 25123 Brescia, Italy
lucia.gastaldi@ing.unibs.it

Key words: Finite Elements, Immersed Boundary Method, Fluid-Structure Interactions, Mass conservation, Fictitious Domain.

Abstract. This research is devoted to mass conservation and CFL properties of the Finite Elements Immersed Boundary Method. We first explore an enhanced higher order scheme applied to the Finite Element Immersed Boundary Method technique introduced by Boffi and Gastaldi. This technique is based on a Pointwise (PW) formulation of the kinematic condition, and higher order elements show better conservation properties than the original scheme. A further improvement with respect to the classical PW formulation is achieved introducing a fully variational Distributed Lagrange Multiplier (DLM) formulation. Numerical experiments show that DLM is not affected by any CFL condition. Furthermore the mass conservation properties of this method are extremely competitive.

1 INTRODUCTION

Several applications require the modeling of fluid structure interactions. In particular, the Immersed Boundary Method (IBM) has been developed to tackle the biomedical modeling of organic tissues. The IBM has been firstly considered by Peskin in the seventies, see [13] for a review.

Boffi and Gastaldi in [3] introduced a finite element version of the IBM which enjoys interesting properties both for practical and theoretical aspects (see [4, 5, 7, 6, 8, 11, 2]).

Interesting investigations concern, in particular, the choice of the time advancing strategy and the mass conservation of the resulting scheme. In this respect, the main contribution of the present work is twofold. From one side, we explore the use of higher order finite element for the approximation of the fluid; from the other side, we examine a different, in a sense more natural, strategy for handling the movement of the immersed structure. Higher order finite elements are constructed extending the ideas of [1] for the enhancement of continuous pressure fluid schemes. The original formulation of the IBM considers a pointwise evolution (PW) of the immersed structure; on the other hand, in this paper we consider a variational formulation of the structure evolution equation (see also [12]). This gives rise to a scheme which shares several analogies with the Fictitious Domain method with Distributed Lagrange Multiplier (see, for instance, [10]); for this reason we shall refer to this scheme as DLM approach.

It turns out that the first modification of the original IBM formulation (higher-order fluid scheme) provides significant improvements of the mass conservation and that the second modification (DLM) gives rise to a scheme which is superior in terms of time advancing procedure (no CFL condition is required for its stability). Surprisingly enough, we observed that the DLM approach enjoys much better mass conservation properties as well, thus becoming a very promising scheme for future studies.

2 PROBLEM SETTING

Let $\Omega \subset \mathbb{R}^d$, $d = 2, 3$ be the fluid domain, and let the structure domain $\mathcal{B}_t \subset \Omega$ be immersed into the fluid one. We consider incompressible fluid and viscoelastic structure. The key assumption of the IBM lays in the particular form of the structure stress tensor. In fact we assume the structure stress tensor to be composed by an elastic and a viscous contribution. The viscous contribution has exactly the same form as for the fluid, then the principle of virtual work applies.

More in detail, at time t the structure lays on the time dependent domain $\mathcal{B}_t$. The structure domain can be parametrized by a map $\mathbf{X}$ on a reference domain $\mathcal{B} \subset \mathbb{R}^m$, $m = d, d-1$. In a Lagrangian framework we set $\mathbf{s}$ as the reference variable in $\mathcal{B}$. A material point on the current domain $\mathcal{B}_t$ is denoted by $\mathbf{x}$. A typical assumption is $\partial\mathcal{B}_t \cap \partial\Omega = \emptyset$. We consider the initial domain as the reference one $\mathcal{B} = \mathcal{B}_0$.

The map $\mathbf{X}$ represents the relationship between the current and the reference domains:

$$\mathbf{X} : \mathcal{B} \times [0, T] \to \mathcal{B}_t \quad \text{so that } \mathbf{x} = \mathbf{X}(\mathbf{s}, t) \ \forall \mathbf{x} \in \mathcal{B}_t. \tag{1}$$

We assume $\mathbf{X}(\mathbf{s}, t)$ being invertible at any time, which implies that the deformation gradient $\mathbb{F}_{\alpha i} := \big(\boldsymbol{\nabla}_s \mathbf{X}(\mathbf{s}, t)\big)_{\alpha i} = \mathbf{X}_{\alpha,i}(\mathbf{s}, t) = \frac{\partial \mathbf{X}_\alpha(\mathbf{s},t)}{\partial s_i}$ has rank m. We have that $|\mathbb{F}| = 1$ at the initial time; thanks to the incompressibility assumption this is true also at any subsequent time. Here $|\mathbb{F}|$ stands for the determinant of $\mathbb{F}$ in the case $m = d$. When $m = d - 1$ we set $|\mathbb{F}| = |\partial\mathbf{X}/\partial s|$ for $m = 1$ and $|\mathbb{F}| = |\partial\mathbf{X}/\partial s_1 \wedge \partial\mathbf{X}/\partial s_2|$ for $m = 2$.

The kinematics of the material particle can be defined through its velocity:

$$\mathbf{u}(\mathbf{x},t)=\frac{\partial \mathbf{X}}{\partial t}(\mathbf{s},t) \quad \text{for } \mathbf{x}=\mathbf{X}(\mathbf{s},t). \tag{2}$$

The densities of the incompressible fluid and solid phases are assumed to be piecewise constant:

$$\rho=\begin{cases} \rho_f & \text{in } \Omega\setminus\mathcal{B}_t \\ \rho_s & \text{in } \mathcal{B}_t. \end{cases} \tag{3}$$

Detailed study of stability criteria regarding the ratio ρ_s/ρ_f can be found in [2]. We already mentioned that the key idea of IBM lays in the definition of the Cauchy stress tensor $\boldsymbol{\sigma}$ as:

$$\boldsymbol{\sigma}=\begin{cases} \boldsymbol{\sigma}_f & \text{in} \quad \Omega\setminus\mathcal{B}_t \\ \boldsymbol{\sigma}_f+\boldsymbol{\sigma}_s & \text{in} \quad \mathcal{B}_t. \end{cases} \tag{4}$$

Here we have the viscous term all over the domain, and the elastic contribution is taken into account where the structure is located. This assumption is accepted in biological frameworks where the viscoelasticity of the tissues play a key role (see, e.g., [14]). The stress tensor for a viscous fluid is:

$$\boldsymbol{\sigma}_f=-p\mathbb{I}+\mu(\nabla\,\mathbf{u}+(\nabla\,\mathbf{u})^T). \tag{5}$$

The first Piola–Kirchhoff stress tensor can be derived from the elastic stress tensor $\boldsymbol{\sigma}_s$ using Lagrangian variables as:

$$\mathbb{P}(\mathbf{s},t)=|\mathbb{F}(\mathbf{s},t)|\,\boldsymbol{\sigma}_s(\mathbf{X}(\mathbf{s},t),t)\,\mathbb{F}^{-T}(\mathbf{s},t). \tag{6}$$

Using the principle of virtual work and equations (3)-(6) we obtain the following formulation of the problem:

Problem 2.1 *Given $\mathbf{u}_0\in H^1_0(\Omega)^d$ and $\mathbf{X}_0:\mathcal{B}\to\Omega$ such that $\mathbf{X}_0\in W^{1,\infty}(\mathcal{B})$, for all $t\in\,]0,T[$, find $(\mathbf{u}(t),p(t))\in H^1_0(\Omega)^d\times L^2_0(\Omega)$ and $\mathbf{X}(t)\in W^{1,\infty}(\mathcal{B})$, such that*

$$\rho_f\frac{d}{dt}(\mathbf{u}(t),\mathbf{v})+b(\mathbf{u}(t),\mathbf{u}(t),\mathbf{v})+a(\mathbf{u}(t),\mathbf{v}) \\ -(\boldsymbol{\nabla}\cdot\mathbf{v},p(t))=\langle\mathbf{d}(t),\mathbf{v}\rangle+\langle\mathbf{F}(t),\mathbf{v}\rangle \qquad \forall\mathbf{v}\in H^1_0(\Omega)^d \tag{7a}$$

$$(\boldsymbol{\nabla}\cdot\mathbf{u}(t),q)=0 \qquad \forall q\in L^2_0(\Omega) \tag{7b}$$

$$\langle\mathbf{d}(t),\mathbf{v}\rangle=-(\rho_s-\rho_f)\int_{\mathcal{B}}\frac{\partial^2\mathbf{X}}{\partial t^2}\mathbf{v}(\mathbf{X}(\mathbf{s},t))\,d\mathbf{s} \qquad \forall\mathbf{v}\in H^1_0(\Omega)^d \tag{7c}$$

$$\langle\mathbf{F}(t),\mathbf{v}\rangle=-\int_{\mathcal{B}}\mathbb{P}(\mathbb{F}(\mathbf{s},t)):\nabla_s\mathbf{v}(\mathbf{X}(\mathbf{s},t))\,d\mathbf{s} \qquad \forall\mathbf{v}\in H^1_0(\Omega)^d \tag{7d}$$

$$\frac{\partial\mathbf{X}}{\partial t}(\mathbf{s},t)=\mathbf{u}(\mathbf{X}(\mathbf{s},t),t) \qquad \forall\mathbf{s}\in\mathcal{B} \tag{7e}$$

$$\mathbf{u}(\mathbf{x},0)=\mathbf{u}_0(\mathbf{x}) \qquad \forall\mathbf{x}\in\Omega \tag{7f}$$

$$\mathbf{X}(\mathbf{s},0)=\mathbf{X}_0(\mathbf{s}) \qquad \forall\mathbf{s}\in\mathcal{B}. \tag{7g}$$

We have used the following definitions for the bilinear forms

$$a(\mathbf{u},\mathbf{v}) = \mu(\boldsymbol{\nabla}_{sym}\,\mathbf{u}, \boldsymbol{\nabla}_{sym}\,\mathbf{v}),$$
$$b(\mathbf{u},\mathbf{v},\mathbf{w}) = \frac{\rho_f}{2}\left((\mathbf{u}\cdot\boldsymbol{\nabla}\,\mathbf{v},\mathbf{w}) - (\mathbf{u}\cdot\boldsymbol{\nabla}\,\mathbf{w},\mathbf{v})\right),$$

where $\boldsymbol{\nabla}_{sym}\,\mathbf{u} = (\boldsymbol{\nabla}\,\mathbf{u} + (\boldsymbol{\nabla}\,\mathbf{u})^T)/2$.
We observe that in the above formulation we have that the incompressible Navier–Stokes equations (7a)-(7b) are written in variational form, while the movement of the structure governed by (7e) is written pointwise, since at each point $\mathbf{s} \in \mathcal{B}$ we solve an ordinary differential equation with initial value given by (7g). For this reason we address this formulation as PW in the rest of the paper.

We assume that the structure is composed by a hyperelastic material. These materials are characterized by a positive energy density $W(\mathbb{F})$ depending only on the deformation gradient. Then the first Piola–Kirchhoff stress tensor $\mathbb{P}$ can be expressed in terms of the potential energy density as $(\mathbb{P}(\mathbb{F}(\mathbf{s},t))_{\alpha i} = \partial W(\mathbb{F}(\mathbf{s},t))/\partial\mathbb{F}_{\alpha i}$ where $i = 1,\dots,m$ and $\alpha = 1,\dots,d$; the elastic potential energy of the body is given by:

$$E\left(\mathbf{X}(t)\right) = \int_{\mathcal{B}} W(\mathbb{F}(s,t))\mathrm{d}\mathbf{s}.$$

Assuming that the potential energy density W is convex, that $\rho_s \geq \rho_f$, and using the relation between the energy density and the Piola–Kirchhoff above, the following energy estimate can be obtained for all $t \in [0,T]$:

$$\frac{\rho_f}{2}\frac{d}{dt}||\mathbf{u}(t)||_0^2 + \mu||\,\nabla\,\mathbf{u}(t)||_0^2 + \frac{\rho_s-\rho_f}{2}\frac{d}{dt}\left\|\frac{\partial\mathbf{X}}{\partial t}\right\|_{0,\mathcal{B}}^2 + \frac{d}{dt}E(\mathbf{X}(t)) = 0. \tag{8}$$

In the following section we present the space-time discretization of Problem 2.1 based on the use of finite elements, and in the next one we shall introduce a variational version also of equation (7e). The issue of the stability for the space-time scheme will be also addressed.

3 MASS PRESERVING HIGH ORDER FINITE ELEMENT SPACES

In this section we discretize Problem 2.1 using high order mass preserving stable finite elements. Consider a triangulation $\mathcal{T}_h$ of Ω into triangles or rectangles if $d = 2$, and tetrahedrons or parallelepipeds if $d = 3$. We denote by K any single element of $\mathcal{T}_h$.

The structure domain $\mathcal{B}$ is subdivided into segments, triangles or tetrahedrons for $m = 1, 2, 3$ respectively; we denote this subdivision by $\mathcal{S}_h$. We shall need also the following notation: T_k, $k = 1,\dots,M_e$ is an element of $\mathcal{S}_h$, $\mathbf{s}_j$, $j = 1,\dots,M$ stands for a vertex of $\mathcal{S}_h$, and $\mathcal{E}_h$ is the set of the edges (or faces) e of $\mathcal{S}_h$. Given these definitions we introduce the solution space for the structure position S_h:

$$S_h = \{\mathbf{Y} \in C^0(\mathcal{B};\Omega): \quad \mathbf{Y}|_{T_k} \in P_1(T_k)^d,\ k = 1,\dots,M_e\}, \tag{9}$$

being $P_1(T_k)$ the space of affine polynomials on the element T_k.

As far as the fluid domain is concerned, we consider two finite dimensional spaces $V_h \subseteq H_0^1(\Omega)^d$ and $Q_h \subseteq L_0^2(\Omega)$ for the velocity and pressure discretizations, respectively. It is well know that these two spaces need to satisfy the inf-sup condition [9]. We recall also that, due to the presence of the source term localized along the structure, the pressure might present jumps along the interface between fluid and solid. For this reason, pairs of finite element spaces enjoying the so called *local mass conservation* property are to be preferred. Discontinuous pressure schemes enjoy this property, however many popular Stokes elements, as e.g. Hood–Taylor and Bercovier–Pironneau elements, are based on continuous pressure. In [1] we proposed and analyzed an enhancement of such elements by adding to the pressure space piecewise constant functions. In this work we consider higher polynomial degree and higher enhancing shape functions with respect to [1]. More precisely, we consider the Hood–Taylor element of degree 2, that is the velocities are piecewise cubic polynomials while the pressures are continuous piecewise quadratic. Then we add to the pressure space discontinuous piecewise affine functions. Hence the resulting two-dimensional finite element spaces are:

$$\begin{aligned} V_h &= \{\mathbf{v} \in H_0^1(\Omega)^d : \mathbf{v}|_K \in P_3(K)^d\ \forall K \in \mathcal{T}_h\} \\ Q_h &= \{q \in L_0^2(\Omega) : q = q_2 + q_1,\ q_2 \in C^0(\bar\Omega), \\ &\qquad q_2|_K \in P_2(K),\ q_1|_K \in P_1(K)\ \forall K \in \mathcal{T}_h\}. \end{aligned} \tag{10}$$

Let us introduce a subdivision of the interval $(0,T)$ in N equal parts with size Δt, then $t_n = n\Delta t$ and $\mathbf{u}^n$ stands for the value of the function $\mathbf{u}$ at time t_n. Similar notation holds for the other functions involved in the problem. Applying a modified backward Euler scheme to equations (7a)-(7b) and (7e) and using the latter in order to discretize the source term (7c) we end up with the following time advancing scheme.

Step 1. Compute

$$\langle \mathbf{F}_h^{n+1}, \mathbf{v}\rangle = -\sum_{e\in\mathcal{E}_h} [\![\mathbb{P}_h]\!]^n \cdot \mathbf{v}(\mathbf{X}_h^n(s,t))\,\mathrm{dA} \qquad \forall \mathbf{v} \in V_h. \tag{11}$$

Step 2. Solve the Navier–Stokes equations: find $(\mathbf{u}_h^{n+1}, p_h^{n+1}) \in V_h \times Q_h$ such that

$$\begin{aligned} &\rho_f\left(\frac{\mathbf{u}_h^{n+1}-\mathbf{u}_h^n}{\Delta t}, \mathbf{v}\right) + b(\mathbf{u}_h^{n+1}, \mathbf{u}_h^{n+1}, \mathbf{v}) + a(\mathbf{u}_h^{n+1}, \mathbf{v}) - (\boldsymbol{\nabla}\cdot\mathbf{v}, p_h^{n+1}) = \\ &\quad -(\rho_s-\rho_f)\int_{\mathcal{B}} \frac{\mathbf{u}_h^{n+1}(\mathbf{X}_h^n(s)) - \mathbf{u}_h^n(\mathbf{X}_h^{n-1}(s))}{\Delta t}\cdot\mathbf{v}(\mathbf{X}_h^n(s))\mathrm{ds} + \langle \mathbf{F}_h^{n+1}, \mathbf{v}\rangle \quad \forall \mathbf{v} \in V_h \end{aligned} \tag{12}$$

$$(\boldsymbol{\nabla}\cdot\mathbf{u}_h^{n+1}, q) = 0 \qquad \forall q \in Q_h.$$

Step 3. Advance the position of the points of the structure:

$$\frac{\mathbf{X}_{hi}^{n+1}-\mathbf{X}_{hi}^{n}}{\Delta t}=\mathbf{u}_h^{n+1}(\mathbf{X}_{hi}^{n})\quad\forall i=1,\dots,M. \tag{13}$$

We remark here that the expression we have introduced to compute the force (7d) takes into account the fact that $\mathbf{X}_h$ is piecewise affine so that $\mathbb{P}(\mathbb{F})$ is piecewise constant.

The space-time scheme described above satisfies an energy estimate similar to (8) provided the following CFL condition is verified

$$\mu-\kappa_{max}C\frac{h_s^{(m-2)}\Delta t}{h_x^{(d-1)}}L^nC_e^n\geq 0 \tag{14}$$

where $L^n:=\max_{T_k\in S_h}\left\{\max_{\mathbf{s}_j,\mathbf{s}_i\in V(T_k)}|\mathbf{X}_{hj}^n-\mathbf{X}_{hi}^n|\right\}$.

4 DISTRIBUTED LAGRANGE MULTIPLIER FORMULATION

In the PW approach we advance the structure moving each point according to equation (7e). We introduce now a different variational approach whose time-space discretization seems to enjoy better stability conditions.

First of all we write equation (7e) in weak form as follows:

$$\left\langle\boldsymbol{\mu},\mathbf{u}(\mathbf{X}(\cdot,t),t)-\frac{\partial\mathbf{X}(\cdot,t)}{\partial t}\right\rangle=0\quad\forall\boldsymbol{\mu}\in(H^1(\mathcal{B})^d)^* \tag{15}$$

where $\langle\cdot,\cdot\rangle$ denotes the duality pairing between $H^1(\mathcal{B})^d$ and its dual space $(H^1(\mathcal{B})^d)^*$. The notation $(\cdot,\cdot)_{\mathcal{B}}$ stands for the L^2-scalar product in $L^2(\mathcal{B})$. Then introducing a Lagrange multiplier associated to the above constraint, Problem 2.1 can be reformulated as follows:

Problem 4.1 *Given $\mathbf{u}_0\in H_0^1(\Omega)^d$ and $\mathbf{X}_0\in W^{1,\infty}(\mathcal{B})$, find $(\mathbf{u}(t),p(t))\in H_0^1(\Omega)^d\times L_0^2(\Omega)$, $\mathbf{X}(t)\in W^{1,\infty}(\mathcal{B})$, and $\boldsymbol{\lambda}(t)\in((H^1(\mathcal{B}))^d)^*$, such that for almost every $t\in]0,T[$ it holds*

$$\rho_f\frac{d}{dt}(\mathbf{u}(t),\mathbf{v})+b(\mathbf{u}(t),\mathbf{u}(t),\mathbf{v})+a(\mathbf{u}(t),\mathbf{v})$$
$$-(\boldsymbol{\nabla}\cdot\mathbf{v},p(t))+\langle\boldsymbol{\lambda}(t),\mathbf{v}(\mathbf{X}(\cdot,t))\rangle=0\qquad\forall\mathbf{v}\in H_0^1(\Omega)^d \tag{16a}$$
$$(\boldsymbol{\nabla}\cdot\mathbf{u}(t),q)=0\qquad\forall q\in L_0^2(\Omega) \tag{16b}$$
$$(\rho_s-\rho_f)\left(\frac{\partial^2\mathbf{X}}{\partial t^2}(t),\mathbf{Y}\right)_{\mathcal{B}}+(\mathbb{P}(\mathbb{F}(t)),\boldsymbol{\nabla}_s\mathbf{Y})_{\mathcal{B}}-\langle\boldsymbol{\lambda}(t),\mathbf{Y}\rangle=0\quad\forall\mathbf{Y}\in(H^1(\mathcal{B}))^d \tag{16c}$$
$$\left\langle\boldsymbol{\mu},\mathbf{u}(\mathbf{X}(\cdot,t),t)-\frac{\partial\mathbf{X}(\cdot,t)}{\partial t}\right\rangle=0\qquad\forall\boldsymbol{\mu}\in((H^1(\mathcal{B}))^d)^* \tag{16d}$$
$$\mathbf{u}(0)=\mathbf{u}_0\quad\text{in }\Omega,\qquad\mathbf{X}(0)=\mathbf{X}_0\quad\text{in }\mathcal{B}. \tag{16e}$$

We consider $\Lambda_h=\{\boldsymbol{\mu}\in C^0(\mathcal{B};\Omega):\boldsymbol{\mu}|_{T_k}\in P_1(T_k)^d,\ k=1,\dots,M_e\}$; then the space-time discretization of Problem 4.1, obtained by approximating the time derivatives in (7a), (16c) and (16d) with proper finite differences, reads:

Problem 4.2 *Given* $\mathbf{u}_{0,h} \in V_h$ *and* $\mathbf{X}_{0,h} \in S_h$*, for* $n = 1, \dots, N$ *find*

$$(\mathbf{u}_h^n, p_h^n) \in V_h \times Q_h, \quad \mathbf{X}_h^n \in S_h, \quad \boldsymbol{\lambda}_h^n \in \Lambda_h,$$

such that $\mathbf{u}_h^0 = \mathbf{u}_{0,h}$, $\mathbf{X}_h^0 = \mathbf{X}_{0,h}$ *and*

$$\begin{aligned}
&\rho_f \left(\frac{\mathbf{u}_h^{n+1} - \mathbf{u}_h^n}{\Delta t}, \mathbf{v} \right) + b(\mathbf{u}_h^{n+1}(t), \mathbf{u}_h^{n+1}(t), \mathbf{v}) + a(\mathbf{u}_h^{n+1}, \mathbf{v}) \\
&\qquad - (\boldsymbol{\nabla}\cdot \mathbf{v}, p_h^{n+1}) + \langle \boldsymbol{\lambda}_h^{n+1}, \mathbf{v}(\mathbf{X}_h^n) \rangle = 0 && \forall \mathbf{v} \in V_h \\
&(\boldsymbol{\nabla}\cdot \mathbf{u}_h^{n+1}, q) = 0 && \forall q \in Q_h \\
&(\rho_s - \rho_f) \left(\frac{\mathbf{X}_h^{n+1} - 2\mathbf{X}_h^n + \mathbf{X}_h^{n-1}}{\Delta t^2}, \mathbf{Y} \right)_{\mathcal{B}} + (\mathbb{P}(\mathbb{F}_h^{n+1}), \boldsymbol{\nabla}_s \mathbf{Y})_{\mathcal{B}} \\
&\qquad - \langle \boldsymbol{\lambda}_h^{n+1}, \mathbf{Y} \rangle = 0 && \forall \mathbf{Y} \in S_h \\
&\left\langle \boldsymbol{\mu}, \mathbf{u}_h^{n+1}(\mathbf{X}_h^n) - \frac{\mathbf{X}_h^{n+1} - \mathbf{X}_h^n}{\Delta t} \right\rangle = 0 && \forall \boldsymbol{\mu} \in \Lambda_h.
\end{aligned}$$

We remark that in Problem 4.2 we have evaluated the nonlinear terms involving the position of the structure at the previous time. It remains only one possible nonlinear contribution which depends on the expression of $\mathbb{P}$. For clearness we write the time advancing scheme in matrix form in the linear case $\mathbb{P}(\mathbb{F}) = \kappa\mathbb{F}$. Consider time $t^n = n\Delta t$ and solve for t^{n+1}:

$$\begin{pmatrix}
(\frac{\rho_f}{\Delta t} M_u + A) & B^\top & 0 & G(\mathbf{X}_h^n)^\top \\
B & 0 & 0 & 0 \\
0 & 0 & \frac{\delta\rho}{\Delta t^2} M_X + K & -J^\top \\
G(\mathbf{X}_h^n) & 0 & \frac{1}{\Delta t} J & 0
\end{pmatrix}
\begin{pmatrix}
\mathbf{u}_h^{n+1} \\ p_h^{n+1} \\ \mathbf{X}_h^{n+1} \\ \boldsymbol{\lambda}_h^{n+1}
\end{pmatrix}
=
\begin{pmatrix}
\frac{\rho_f}{\Delta t} M_u \mathbf{u}_h^n \\ 0 \\ \frac{\delta\rho}{\Delta t^2} M_X (2\mathbf{X}_h^n - \mathbf{X}_h^{n-1}) \\ \frac{1}{\Delta t} J \mathbf{X}_h^n
\end{pmatrix}$$

with the following definitions of the involved matrices:

M_u, M_X	fluid and structure mass matrices,
A	matrix associated to the convective term and the fluid stiffness,
$G(\mathbf{X})$	matrix associated to $\langle \boldsymbol{\mu}, \mathbf{v}(\mathbf{X}) \rangle$,
B	matrix associated to the divergence,
K	structure stiffness matrix,
J	matrix associated to $\langle \boldsymbol{\mu}, \mathbf{Y} \rangle$.

5 NUMERICAL EXPERIMENTS

In this section we provide numerical experiments illustrating the techniques depicted in this work. We first control the performances of the high order enhanced finite elements defined in (10), both in terms of approximation and local mass conservation. We start with the PW scheme described in Sect. 3. A typical test case for IBM is the simulation of an immersed co-dimension one elastic string. In this case we take $\mathbb{P} = \kappa\mathbb{F}$. The domain

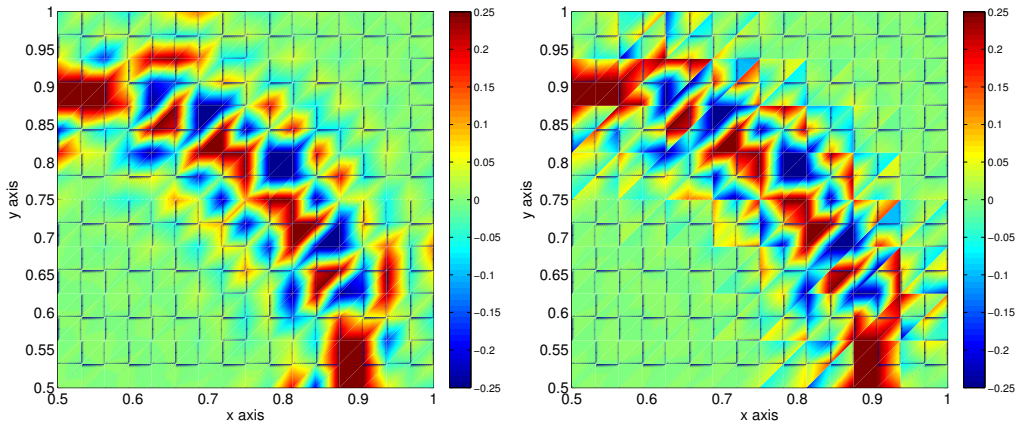

(a) $p - p_h$, P_3/P_2.

(b) $p - p_h$, $P_3/(P_2 + P_0)$.

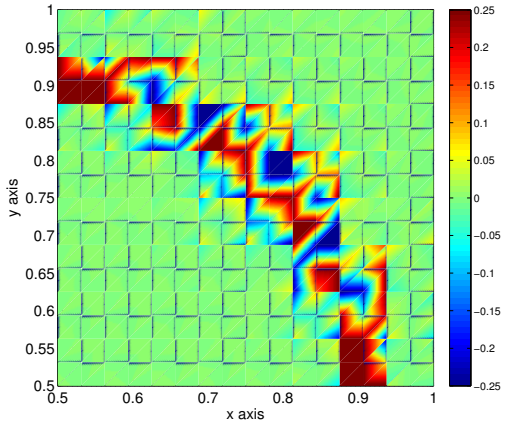

(c) $p - p_h$, $P_3/(P_2 + P_1)$.

Figure 1: Stationary solution for an elastic circle immersed into the fluid, error for the pressure. In the pictures we plot only the upper right corner of the solution.

Ω is the unit square and we a consider a regular mesh obtained by dividing the unit square domain into $N \times N$ squares subdivided into two triangles, with mesh size h_x. The reference domain $\mathcal{B}$ is the unit interval divided into M subintervals with size h_s. When the initial configuration of the string is circular, we have an analytical solution, characterized by a discontinuous pressure, the interested reader can refer to [8] for the details. In Fig. 1, we represent the error distribution for the pressure in the upper right quarter of the domain. In order to visually stress the differences among the different finite element performances we represent the error on a coarse mesh obtained by dividing Ω into 16×16 squares. Due to the discontinuity of the pressure one can appreciate oscillations around the position of the immersed elastic string which can be interpreted as a sort of Gibbs phenomenon. In the case of P_3/P_2 finite element (the standard Hood–Taylor element of degree 2), the area involved by the Gibbs oscillations covers more than three sub-squares

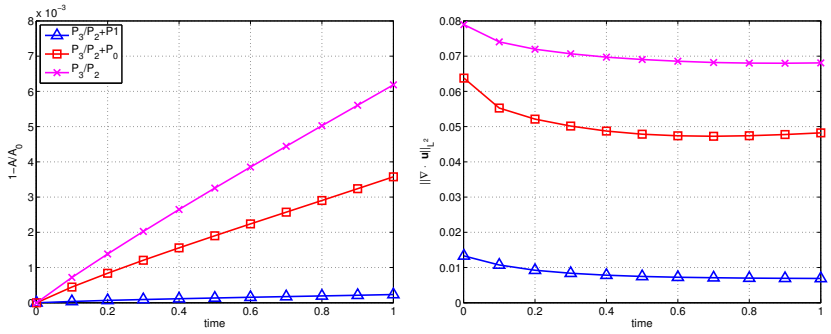

(a) Area conservation for different finite elements.

(b) L^2-norm for the real divergence.

Figure 2: Area conservation, and L^2-norm of the real divergence for the PW scheme with $\kappa = 1$, $\Delta t = 10^-3$, $\mu = 1$, $h_s = 1/1024$, $h_x = 1/16$.

close to the immersed boundary. In the case of the enhancement with piecewise constants $P_3/(P_2+P_0)$, this area is reduced to two or three times h_x, and the error profile is sharper. The enhancement with discontinuous piecewise affine polynomials $P_3/(P_2+P_1)$ provides oscillations greater than 0.1 confined in the same element where the structure is located.

In the second experiment we consider an elastic string whose initial configuration consists of an ellipse. In this case the elastic structure evolves into a circle. Due to the incompressibility constraint the area internal to the elastic boundary has to remain constant, see [4] for details. In Fig. 2 we compare the evolution of the area and of the L^2-norm of the divergence with respect to time. In Fig. 2(a) we see that the enhancement with piecewise constant discontinuous functions is already effective in improving the area conservation, but far more effective is the enhancement with discontinuous piecewise affine polynomials. Same comments hold true for the L^2-norm of the divergence presented in Fig. 2(b). These results suggest that there is a correspondence between the L^2-norm of the divergence and the area preservation of the method.

The next set of experiments is devoted to the comparison between PW and DLM schemes when the $P_3/(P_2+P_1)$ element is used. In Fig. 3 we compare the mass conservation properties of the two schemes. We have used here the same parameters for the two methods and it is evident that the DLM scheme behaves better from this point of view. This fact is also confirmed in Fig. 4 where the position of the structure during a very coarse simulation is shown. The plot of the elastic membrane at subsequent simulation times, demonstrates that, even with a coarse mesh for the structure, the DLM approach can achieve good mass preservation properties, while the PW scheme needs at least one structure point per fluid element. When this last condition is not fulfilled, as in Fig. 4(a), the method fails, and the ellipse collapses instead of setting to a circle.

The next figures illustrate the behavior of PW and DLM schemes from the point of view of the stability. In Sect. 3 we have pointed out that the PW scheme is stable provided the CFL condition (14) is satisfied. Here we show that this condition is no longer required

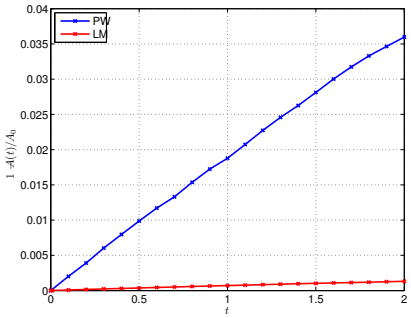

Figure 3: Area conservation for PW and DLM schemes with $\kappa = 1$, $\Delta t = 10^{-2}$, $\mu = 1$, $h_s = 1/1024$, $h_x = 1/32$.

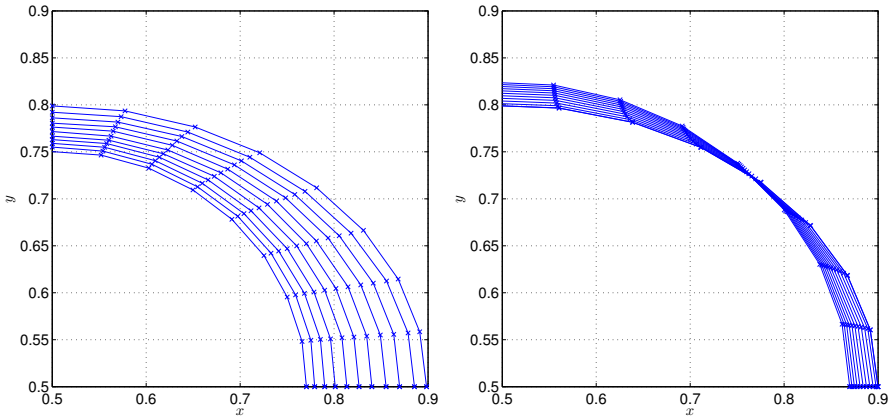

(a) PW. (b) DLM.

Figure 4: Structure position evolving in time.

for the DLM scheme. Fig. 5 reports the energy estimate as a function of time for fixed mesh parameters $h_x = 1/64$ and $h_s = 1/128$ and different values of Δt. We see that the energy of the PW scheme blows up when Δt is greater than 10^{-2} according with (14) while in the DLM scheme it remains constant. Same remark holds also for Fig. 5 where we have fixed $\Delta t = 10^{-2}$ and $h_x = 1/64$ and keep varying h_s.

6 CONCLUSIONS

Higher order enhanced finite elements enjoy area and approximation properties that are up to ten times better in terms of area conservation, and three times better in terms of Gibbs phenomenon controlling (with respect to standard low order elements). Moreover, enhancing with P_1 pressures is much more effective than with P_0. This means that not only it is important to capture the discontinuity in the pressure, but it is also important the accuracy of the functions capturing the pressure discontinuity.

On the other hand, first results related to the DLM formulation are extremely encour-

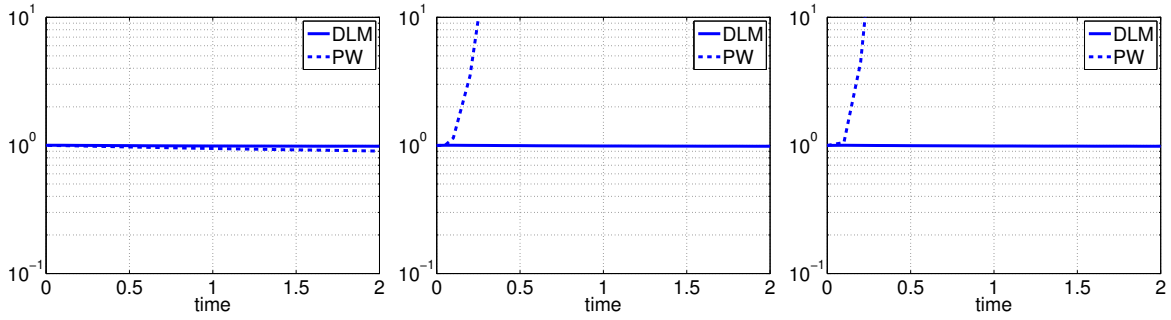

(a) $\Delta t = 10^{-2}$, $\kappa = 5$, $\mu = 1$. (b) $\Delta t = 5.0\ 10^{-2}$, $\kappa = 5$, $\mu = 1$. (c) $\Delta t = 10^{-1}$, $\kappa = 5$, $\mu = 1$.

Figure 5: Ellipse test case. Energy estimations for different Δt, with fixed $\rho = 1$, $\mu = 1$, and $\kappa = 5$. Eulerian mesh size is $h_x = 1/64$, Lagrangian mesh size is $h_s = 1/128$.

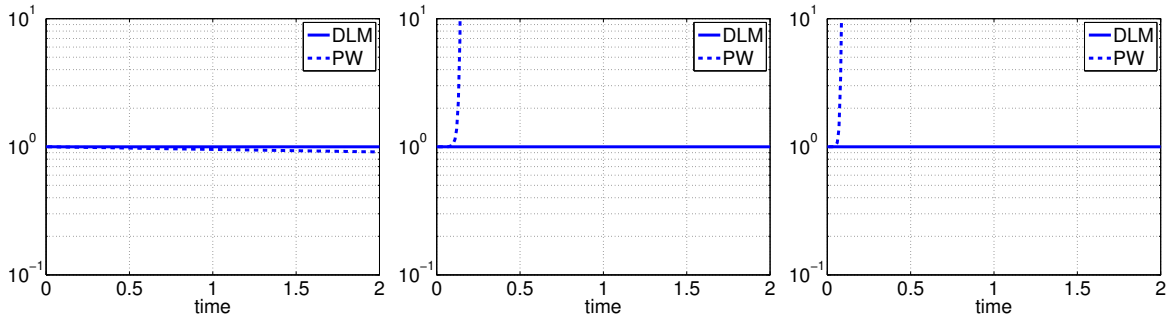

(a) $h_s = 1/128$, $h_x = 1/64$. (b) $h_s = 1/256$, $h_x = 1/64$. (c) $h_s = 1/512$, $h_x = 1/64$.

Figure 6: Ellipse test case. Energy estimations for different h_s, with fixed $\rho = 1$, $\mu = 1$, and $\kappa = 5$, $\Delta t = 10^{-2}$. Eulerian mesh size is $h_x = 1/64$.

aging both in terms of CFL stability and in terms of mass preservation. In fact these results suggest that the performances are worth the implementation and computational price of introducing the Lagrange multiplier for the kinematic condition. These preliminary results will undergo a more extensive and detailed exploration.

REFERENCES

[1] D. Boffi, N. Cavallini, F. Gardini, and L. Gastaldi. Local mass conservation of Stokes finite elements. *J. Sci. Comput.*, 52(2):383–400, 2012.

[2] D. Boffi, N. Cavallini, and L. Gastaldi. Finite element approach to immersed boundary method with different fluid and solid densities. *Math. Models Methods Appl. Sci.*, 21(12):2523–2550, 2011.

[3] D. Boffi and L. Gastaldi. A finite element approach for the immersed boundary method. *Comput. & Structures*, 81(8-11):491–501, 2003. In honour of Klaus-Jürgen Bathe.

[4] D. Boffi, L. Gastaldi, and L. Heltai. A finite element approach to the immersed boundary method. In Scotland Saxe-Coburg Publications, Stirling, editor, *Progress in Engineering Computational Technology, B.H.V. Topping and C.A. Mota Soares Eds.*, pages 271–298, 2004.

[5] D. Boffi, L. Gastaldi, and L. Heltai. Stability results and algorithmic strategies for the finite element approach to the immersed boundary method. In *Numerical mathematics and advanced applications*, pages 575–582. Springer, Berlin, 2006.

[6] D. Boffi, L. Gastaldi, and L. Heltai. Numerical stability of the finite element immersed boundary method. *Math. Models Methods Appl. Sci.*, 17(10):1479–1505, 2007.

[7] D. Boffi, L. Gastaldi, and L. Heltai. On the CFL condition for the finite element immersed boundary method. *Comput. & Structures*, 85(11-14):775–783, 2007.

[8] D. Boffi, L. Gastaldi, L. Heltai, and C. S. Peskin. On the hyper-elastic formulation of the immersed boundary method. *Comput. Methods Appl. Mech. Engrg.*, 197(25-28):2210–2231, 2008.

[9] F. Brezzi and M. Fortin. *Mixed and hybrid finite element methods*, volume 15 of *Springer Series in Computational Mathematics*. Springer-Verlag, New York, 1991.

[10] V. Girault, R. Glowinski, and T. W. Pan. A fictitious-domain method with distributed multiplier for the Stokes problem. In *Applied nonlinear analysis*, pages 159–174. Kluwer/Plenum, New York, 1999.

[11] L. Heltai. On the stability of the finite element immersed boundary method. *Comput. & Structures*, 86(7-8):598–617, 2008.

[12] L. Heltai and F. Costanzo. Variational implementation of immersed finite element methods. *Comput. Methods Appl. Mech. Engrg.*, 229/232:110–127, 2012.

[13] C. S. Peskin. The immersed boundary method. In *Acta Numerica 2002*. Cambridge University Press, 2002.

[14] A. Quarteroni, M. Tuveri, and A. Veneziani. Computational vascular fluid dynamics: problems, models and methods. *Comput. Visual Sci.*, 2:163–197, 2000.